Dalton Transactions

ROYAL SOCIETY OF CHEMISTRY

PAPER

View Article Online
View Journal | View Issue

Cite this: *Dalton Trans.*, 2025, **54**, 14322

Photoluminescence and photoredox catalytic properties of cationic Ru(II) polypyridine complexes encapsulated within an InTATB metal–organic framework

Jongseo Kim and Seong Huh *

The nanoscale environment within the void spaces of metal–organic frameworks (MOFs) can significantly influence the photoredox catalytic activity of encapsulated visible-light photoredox catalysts (PCs). To compare two isostructural PC@In-MOF systems, three cationic Ru(II) polypyridine complexes were successfully encapsulated within the mesoscale channels of the anionic framework of InTATB (H_3TATB = 4,4′,4″-*s*-triazine-2,4,6-triyltribenzoic acid), which features a doubly interpenetrated framework structure. This encapsulation yielded three heterogenized visible-light PCs, RuL_3@InTATB, where L = 2,2′-bipyridine (bpy), 1,10-phenanthroline (phen), or 2,2′-bipyrazine (bpz). A simple cation-exchange process partially replaced the NEt_4^+ counter-cations in the as-prepared InTATB with the cationic Ru(II) polypyridine complexes. The $TATB^{3-}$ linker contains a central triazine unit, a strong electron acceptor, which can engage in intermolecular π–π interactions with one of the three ligands of the $[RuL_3]^{2+}$ complexes. This electronic interaction makes InTATB a more favorable MOF host for stabilizing the excited state of Ru(II)* polypyridine complexes, compared to the previously studied isostructural MOF, InBTB (H_3BTB = 1,3,5-benzenetribenzoic acid), which features a central phenyl donor. The photoluminescence (PL) spectra and PL lifetimes of the three RuL_3@InTATB systems were investigated. In all cases, the PL lifetimes were significantly extended compared to those of the corresponding free $[RuL_3]^{2+}$ complexes. The photoredox catalytic activity was evaluated using the aza-Henry reaction of 2-phenyl-1,2,3,4-tetrahydroisoquinoline (THIQ) under visible light at room temperature (RT). The RuL_3@InTATB systems exhibited higher conversion rates and enhanced product selectivity compared to their RuL_3@InBTB counterparts, likely due to their extended PL lifetimes. These heterogenized systems also demonstrated strong catalytic performance in the visible-light-driven aerobic oxidation of benzyl halides in the presence of an auxiliary organocatalyst, also under mild conditions at RT.

Received 11th June 2025,
Accepted 26th August 2025

DOI: 10.1039/d5dt01373a

rsc.li/dalton

1. Introduction

The unique spatial distribution of luminescent chromophores within the preorganized channels of metal–organic frameworks (MOFs) often induces unusual photophysical properties of the encapsulated chromophores due to pore confinement effects.[1–7] During crystal formation, free crystalline chromophore molecules tend to pack closely together, which can lead to self-quenching effects that diminish their emission properties.[8] In contrast, the precise positioning of these luminescent chromophores within well-defined MOF channels can theoretically prevent such detrimental self-quenching pathways, thereby enhancing their emissive properties. Using this straightforward approach, we previously demonstrated that cationic dyes encapsulated within large mesoscale MOF channels exhibit enhanced and/or unique photoluminescence (PL) emission properties.[5–7] Additionally, this concept can be further extended to rationally tailor the photophysical properties and catalytic activities of encapsulated cationic Ru(II) polypyridine photoredox catalysts (PCs), which exhibit excellent visible-light photoredox performance.[9]

Due to their versatility in synthetic organic chemistry, a wide range of organic transformations catalyzed by visible-light-responsive, transition metal-based PCs under mild conditions have attracted significant attention over the past decade.[10–14] To mitigate their high cost, it is essential to develop efficient heterogeneous transition metal-based PC systems with high recyclability. Heterogenized PCs offer the advantage of easy recovery and reuse, while also minimizing

Department of Chemistry and Protein Research Center for Bio-Industry, Hankuk University of Foreign Studies, Yongin 17035, Republic of Korea. E-mail: shuh@hufs.ac.kr; Fax: +8231 330 4566; Tel: +82 31 330 4522

the risk of product contamination from residual metal ions. Several competing heterogenization strategies have been developed for cationic transition metal-based PCs to simultaneously enhance their catalytic activity and recyclability.[9,15–20] [Ru(bpy)$_3$]$^{2+}$ (bpy = 2,2′-bipyridine) is one of the most widely used PCs, owing to its long-lived luminescent triplet metal–ligand charge transfer (^{3}MLCT) excited state under visible light irradiation. Simple adsorption of [Ru(bpy)$_3$]$^{2+}$ onto the surface of nonporous silica nanoparticles (~6 nm) yielded a heterogenized catalyst (denoted as Ru(bpy)$_3$/SiO$_2$), which exhibited significantly enhanced catalytic activity in photooxidation reactions, particularly in the synthesis of pharmaceutically relevant terpene derivatives.[16] In another approach, direct coupling of dibrominated bpy-containing [Ru(bpy)$_3$]$^{2+}$ or [Ir(ppy)$_2$(bpy)]$^+$ (ppy = 2-phenylpyridine) units with tetra(*p*-ethynylphenyl) methane *via* Pd-catalyzed Sonogashira cross-coupling afforded well-defined heterogeneous PCs. These polymeric materials featured [Ru(bpy)$_3$]$^{2+}$ or [Ir(ppy)$_2$(bpy)]$^+$ phosphors integrated into the polymer backbone with high loading.[17]

Very recently, a new encapsulation method reported the use of MOFs as host materials for Ru(II) polypyridine PCs to produce PC@MOFs. For example, [Ru(bpy)$_3$]$^{2+}$ was encapsulated through a cation exchange method using Zr-based PCN-608 MOFs modified with suitable ionic linkers, and Ru(bpy)$_3$@PCN-608-SBDC (H_3SBDC = 2-sulfoterephthalic acid) showed excellent photoredox catalytic activity in the aza-Henry reaction of 2-phenyl-1,2,3,4-tetrahydroisoquinoline (THIQ).[18] Three different Ru(II) polypyridine PCs were also efficiently encapsulated within the anionic framework of the as-prepared InBTB (H_3BTB = 1,3,5-benzenetribenzoic acid) through simple cation exchange.[9] These RuL$_3$@InBTB catalytic systems enhanced the photoredox catalytic activity in the aza-Henry reaction of THIQ, where L = bpy, 1,10-phenanthroline (phen), and 2,2′-bipyrazine (bpz), due to the extended excited states of the Ru(II)* polypyridine species. Additionally, the quantum yields of the encapsulated Ru(II) polypyridine PCs can be improved by minimizing the unfavorable nonradiative decay pathways related to metal-centered d–d transitions by the confinement effect.[21] The RuL$_3$@InBTB catalytic system is also structurally robust for repeated catalyst use.[9] Thus, this straightforward strategy represents an important heterogenization approach for cationic transition metal-based PCs, and similar methods have been successfully applied to heterogenize cationic Ir(III)-based PCs such as [Ir(ppy)$_2$(bpy)]$^+$ and [Ir(tpy)(ppy)Cl]$^+$ (tpy = 2,2′:6′,2″-terpyridine) using ZJU-28 and USF-2, respectively.[19,20]

Despite these recent promising reports on the immobilization of PCs within preorganized MOF channels, a comparative evaluation of the catalytic activities of encapsulated PCs in isostructural MOFs with differing pore functionalities and environments remains unexplored; in this study, we aim to address this gap by fine-tuning the pore properties of MOFs to further enhance the visible-light photoredox activities of encapsulated Ru(II) polypyridine PCs. Owing to the well-developed silane chemistry, pore engineering—*i.e.*, the modulation of pore properties through various organic functionalizations—has become a widely utilized strategy in the development of mesoporous silica materials.[22,23] Similarly, the pore engineering of MOF channels through the incorporation of Lewis basic or acidic functionalities is an attractive strategy for tailoring pore environments on demand, enabling advanced applications such as catalysis, adsorption, gas separation, and biomedical uses.[24] To this end, we prepared an isostructural anionic framework of In-MOF (denoted as InTATB, TATB^{3-} = 4,4′,4″-*s*-triazine-2,4,6-triyltribenzoate) containing a tritopic TATB^{3-} bridging linker, instead of the BTB^{3-} linker in InBTB, based on the literature method.[25] The chemical formula of InTATB is $(Et_4N)_3[In_3(TATB)_4]\cdot(DEF)_{16}\cdot(H_2O)_{11}$. Fig. 1a and b show the doubly interpenetrated anionic framework structure. The tritopic TATB^{3-} bridging linker features a central triazine ring containing three nitrogen atoms, which serve as potentially strong electron-accepting sites.[26,27] Thus, the open channels of InTATB possess well-ordered, strong electron-accepting sites, in contrast to those of InBTB. We anticipated that the regularly arranged triazine moieties would enhance electronic interactions between the anionic framework and the [RuL$_3$]$^{2+}$ guest ions *via* potential intermolecular π–π interactions, thereby improving their PL properties for efficient photoredox catalysis. This feature may make InTATB a more advantageous MOF host for Ru(II) polypyridine PCs, enabling more effective stabilization of their excited states (Ru(II)*) compared to the previously studied isostructural InBTB, which contains a central phenyl donor group.

Herein, UV/vis-absorption spectroscopy was employed to investigate the encapsulation of the three cationic Ru(II) polypyridine PCs shown in Fig. 1c–e. The PL properties of the resulting RuL$_3$@InTATB MOFs were systematically characterized by steady-state fluorescence measurements in the solid

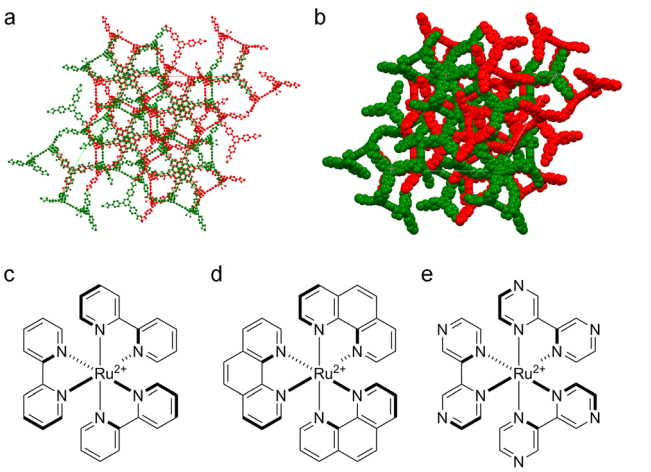

Fig. 1 The crystal structure of a doubly-interpenetrated InTATB framework shown in a ball-and-stick representation (a) and a CPK representation (b) along the *c*-axis. Two catenated frameworks are shown in different colors. Hydrogen atoms, counter-cations, and solvent are omitted for clarity.[25] The chemical structures of the three cationic Ru(II) polypyridine complexes with good visible-light photoredox catalytic activities: (c) [Ru(bpy)$_3$]$^{2+}$, (d) [Ru(phen)$_3$]$^{2+}$, and (e) [Ru(bpz)$_3$]$^{2+}$.

state, and their PL lifetimes were also determined. To evaluate the photoredox catalytic activities, the aza-Henry reaction of THIQ and the aerobic oxidation of benzyl halides were selected as model reactions and compared across RuL_3@InTATB, free $[RuL_3]^{2+}$ ions, and RuL_3@InBTB under visible light irradiation using a commercial compact fluorescent lamp at RT.[9,28]

2. Experimental methods

2.1. Chemicals

All reagents and solvents were of reagent grade and were used as received. $[Ru(bpy)_3]Cl_2$, $[Ru(phen)_3]Cl_2$, $[Ru(bpz)_3][PF_6]_2$, ethyl α-bromophenylacetate, methyl α-bromophenylacetate, methyl (2-chlorophenyl)acetate, methyl (4-chlorophenyl)acetate, ethyl 2-bromo-(4-bromophenyl)acetate, methyl 2-bromo-2-(2-chlorophenyl)acetate, and methyl 2-bromo-2-(4-chlorophenyl) acetate were purchased from Sigma-Aldrich. *N*,*N*-Diethylformamide (DEF) and 1,1,2,2-tetrachloroethane (TCE) were purchased from TCI and were used as received. 4,4′,4″-*s*-Triazine-2,4,6-triyltribenzoic acid (H_3TATB) was supplied by Chemsoon. InTATB, $(Et_4N)_3[In_3(TATB)_4]\cdot(DEF)_{16}\cdot(H_2O)_{11}$, was prepared according to the literature method,[25] while 2-phenyl-1,2,3,4-tetrahydroisoquinoline (THIQ) was also synthesized according to the literature method.[29]

2.2. Encapsulation of cationic Ru(II) polypyridine complexes within InTATB

A solution of $[Ru(bpy)_3]Cl_2$ and $[Ru(phen)_3]Cl_2$ dissolved in 10 mL of ethanol (2 mM) containing 10 mg of the as-prepared InTATB was gently shaken for 5 days. In the case of $[Ru(bpz)_3][PF_6]_2$, acetonitrile was used instead of ethanol. The RuL_3@InTATB solids were retrieved by filtration, washed with the solvent and dried in air at RT.

2.3. Aza-Henry reaction of THIQ with RuL_3@InTATB

THIQ (26.16 mg, 0.125 mmol) was dissolved in 5 mL of reagent-grade nitromethane in a 50 mL round-bottom flask. RuL_3@InTATB equivalent to 2.5×10^{-3} mmol of the Ru(II) polypyridine complex was added to the reaction mixture. After a small magnetic stir bar was added, the round-bottom flask was capped with a rubber septum with a pinhole (syringe needle). The reaction flask was placed at a 10 cm distance from a compact fluorescent lamp (20 W Cool White CFL, GE Edison). The reaction mixture was exposed to light for 48 h. After the reaction, RuL_3@InTATB was separated by centrifugation. The supernatant was transferred to a 250 mL round-bottom flask, while the residual solution was washed with $CHCl_3$. The reaction mixture was evaporated to dryness using a rotary evaporator and dried under high vacuum. The residue was dissolved in a small amount of $CDCl_3$, and an internal standard (TCE, 13.2 μL, 0.125 mmol) was added. The substrate conversion and product yield were measured by ^{1}H NMR spectroscopy. The recycling test was conducted using $Ru(bpy)_3$@InTATB under identical reaction conditions.

2.4. Aerobic oxidation of benzyl halides with RuL_3@InTATB

A benzyl halide of choice (0.2 mmol), 4-methoxypyridine (4 μL, 0.04 mmol), and Li_2CO_3 (0.0148 g, 0.2 mmol) were dissolved in 1 mL of reagent-grade dimethylacetamide (DMA) in a 50 mL round-bottom flask. RuL_3@InTATB equivalent to 2.0×10^{-3} mmol of the Ru(II) polypyridine complex was added to the reaction mixture. After a small magnetic stir bar was added, the round-bottom flask was capped with a rubber septum with a pinhole (syringe needle). The reaction flask was placed at a 5 cm distance from a compact fluorescent lamp (20 W Cool White CFL, GE Edison). The reaction mixture was exposed to light for 48 h. After the reaction, RuL_3@InTATB was separated by centrifugation. DMA (9 mL) was added to the supernatant, and ethyl acetate (30 mL) and deionized water (30 mL) were also added. The organic phase was separated. The extraction was repeated three more times using ethyl acetate (50 mL). The combined organic phase was washed with a brine solution (25% NaCl) three times. The organic phase was dried using anhydrous $MgSO_4$. After filtration, the dried organic phase was evaporated to dryness using a rotary evaporator and dried under high vacuum. The residue was dissolved in a small amount of $CDCl_3$, and TCE (21.1 μL, 0.2 mmol) was added. The substrate conversion and product yield were measured by ^{1}H NMR spectroscopy.

2.5. Physical measurements

NMR spectra were recorded using a Bruker Ascend 400 (400.13 MHz for ^{1}H) spectrometer. The proton chemical shifts of the samples were calibrated with respect to the reference proton resonance signals emitted from the protic residues of the deuterated solvents. The elemental composition of the MOF sample was analyzed at the Organic Chemistry Research Center (Seoul, Korea). UV/vis-absorption spectra were collected using a Scinco S-3100 spectrophotometer. Solid-state fluorescence spectra were collected using a Hitachi F-4500 fluorescence spectrophotometer. Cyclic voltammetry was performed on a CompactStat potentiostat/galvanostat (Ivium Technologies, Netherlands). Cyclic voltammograms were recorded using a glassy carbon working electrode (CHI104, O. D. 6.35 mm, I.D. 3 mm, CH Instruments, USA), an Ag/AgCl reference electrode (RE-1B, ALS, Japan), and a Pt wire counter electrode in 0.1 mM $TEABF_4$ acetonitrile solution. A small amount of solid sample was directly put on a glassy carbon electrode, covered with a drop of Nafion-117 solution (Sigma-Aldrich), and dried at RT for 2 h. The voltage was applied in the following manner: 0 V → 2.5 V → −2.5 V → 0 V. The scan rate was 20 mV s^{-1}. The CV curves were cycled four times, and the second CV curve was used to calculate the redox potential.

2.6. Photoluminescence lifetime measurements

Time-resolved photoluminescence (TRPL) imaging was performed by inverted scanning confocal microscopy (MicroTime-200, Picoquant, Germany) with a 60× (water) objective. The measurements were performed at the Korea Basic Science Institute, Daegu Center. A single-mode pulsed diode laser

(470 nm with an ~30 ps pulse width and an average power of <1 μW) was used as an excitation source. A dichroic mirror (490 DCXR, AHF), a long-pass filter (HQ500lp, AHF), and a single-photon avalanche diode (SPAD; PDM series, MPD) were used to collect the emission data from each sample. A time-correlated single-photon counting technique was used to count the photons emitted. TRPL images with dimensions of 80 μm × 80 μm, consisting of (200 × 200) pixels, were recorded using a time-tagged time-resolved (TTTR) data acquisition route. The acquisition time for each pixel was 2 ms. The obtained PL decays were exponentially fitted using SymPhoTime-64 software.

3. Results and discussion

3.1. Preparation of RuL_3@InTATB

To obtain a closely related MOF system with identical pore geometry but distinct pore environments for encapsulating $[RuL_3]^{2+}$ ions, the InTATB framework—an isostructural analogue of InBTB—was synthesized following a reported procedure.[25] The tritopic $TATB^{3-}$ linker features a central triazine ring in place of the phenyl ring present in the BTB^{3-} linker. Both InTATB and InBTB crystallize in the same crystal system, exhibiting only slight differences in their unit cell dimensions.[9,25] The counter-cation, $[Et_4N]^+$, was added to the reaction mixture to prepare InTATB. Thus, the main counter-cation in InTATB is $[Et_4N]^+$, instead of the $[Et_2NH_2]^+$ found in InBTB. Three RuL_3@InTATB MOFs (L = bpy, phen, and bpz) were prepared through a cation-exchange process at RT using $[RuL_3]^{2+}$ ions dissolved in ethanol or acetonitrile. Some of the NEt_4^+ counter-cations of InTATB with anionic frameworks were effectively exchanged with the cationic Ru(II) polypyridine complexes. Fig. 2 shows the typical reddish color of $[RuL_3]^{2+}$ ions that the resulting RuL_3@InTATB exhibited.

Fig. 3 shows that the encapsulation process was periodically monitored by analyzing the aliquot by UV/vis-spectroscopy, while Table S1 (SI) summarizes the final encapsulation amounts of $[RuL_3]^{2+}$ ions after 5 days. The uptake amounts range from 0.38 to 0.55 μmol mg^{-1} of solid. These uptake amounts are slightly more than those of the RuL_3@InBTB cases.[9] The uptake amounts of $[Ru(bpy)_3]^{2+}$, $[Ru(phen)_3]^{2+}$, and $[Ru(bpz)_3]^{2+}$ were found to be 0.33, 0.42, and 0.42 μmol mg^{-1} of solids, respectively, for RuL_3@InBTB.

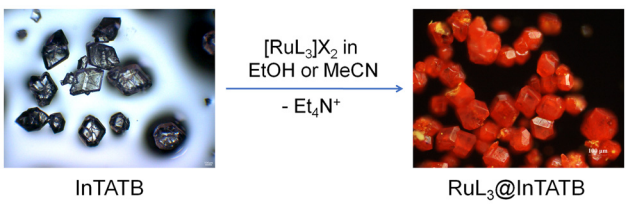

Fig. 2 The illustration of the encapsulation of Ru(II) polypyridine guest ions with InTATB to afford three RuL_3@InTATB MOFs. In this case, the dark field microscopy image of $Ru(bpy)_3$@InTATB is shown.

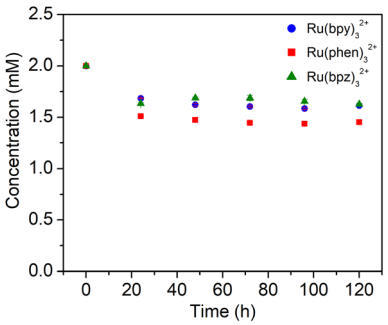

Fig. 3 Time-dependent encapsulation profiles of $[Ru(bpy)_3]^{2+}$ and $[Ru(phen)_3]^{2+}$ by the as-prepared InTATB in EtOH. $[Ru(bpz)_3]^{2+}$ was encapsulated in acetonitrile. Each measurement was repeated in triplicate.

The microscopy investigation implies that the cation-exchange occurred efficiently in the InTATB system, like the previous InBTB system. Fig. S1 (SI) shows the low-magnification microscopy image of $Ru(bpy)_3$@InTATB, which reveals that all crystals are red in color, which is indicative of the highly uniform encapsulation of $[Ru(bpy)_3]^{2+}$. No crystal displayed the original colorless state of InTATB. The uniform distribution of $[RuL_3]^{2+}$ ions right underneath the surfaces of MOF crystals with penetration depths of a few microns was proven to be ideal for heterogeneous photoredox catalysis.[9] This feature makes the heterogeneous system a cost-effective platform for utilizing expensive Ru(II) polypyridine PCs.

3.2. PL properties of RuL_3@InTATB

The PL properties of various luminescent chromophores confined within MOF channels often exhibit intriguing behaviors.[1–7] In general, MOFs possess well-defined, pre-organized channels that spatially orient encapsulated chromophores in unique arrangements, with variable intermolecular distances between isolated chromophores.[5–7] These unique solid-state arrangements of chromophores often result in distinct PL properties compared to those observed in solution. Meanwhile, the solution state $[Ru(bpy)_3]^{2+}$ can be effectively excited to the ^{1}MLCT excited state by visible light irradiation, followed by a rapid intersystem crossing (ISC) process to produce a luminescent ^{3}MLCT excited state.[30] Under visible light excitation, there is an intense ^{3}MLCT emission band at 620 nm in acetonitrile. The lifetime of the ^{3}MLCT excited state of $[Ru(bpy)_3]^{2+}$ in acetonitrile was reported to be 1100 ns.[12] This long-lived luminescent ^{3}MLCT excited state is well suited to visible-light photoredox catalysis as a reductant or an oxidant. Based on these backgrounds, the solid-state PL properties of the samples were investigated by steady-state fluorescence spectroscopy at RT to compare the PL properties of the newly prepared RuL_3@InTATB with the previous RuL_3@InBTB.

Generally, the MLCT-based absorption and emission band maxima of $[Ru(bpy)_3]^{2+}$ ions are solvent-dependent in solution. Caspar and Meyer systematically investigated the solvent-dependence of the energy of the emission band maxima and

the lifetimes of $[Ru(bpy)_3]^{2+}$ ions dissolved in various solvents.[31] A polar solvent induced red-shifted emission band maxima. In addition, higher solvent polarity resulted in shorter emission lifetimes. The RuL_3@InTATB MOF crystals were not ground prior to measurements to prevent partial framework collapse and potential leaching of the $[RuL_3]^{2+}$ ions. Fig. 4 shows the resulting PL spectra. All RuL_3@InTATB MOFs show a characteristic ^{3}MLCT-based solid-state PL emission band from a strong ^{3}MLCT-based emission. Ru(bpy)$_3$@InTATB (λ_{em} = 599 nm, λ_{ex} = 450 nm) shows almost the same maximum PL emission band position, or energy of the emission maximum, with Ru(bpy)$_3$@InBTB (λ_{em} = 598 nm, λ_{ex} = 450 nm). Since this emission band position is closely related to the free energy content of the excited state (ΔG_{ES}) to calculate the redox potential of the excited Ru(II)* species,[32–34] very similar emission band positions of Ru(bpy)$_3$@InTATB and Ru(bpy)$_3$@InBTB imply that their redox potentials for the excited Ru(II)* species are similar to one another. On the other hand, Ru(phen)$_3$@InTATB (λ_{em} = 596 nm, λ_{ex} = 422 nm) showed a blue-shifted PL emission band, compared to Ru(phen)$_3$@InBTB (λ_{em} = 604 nm, λ_{ex} = 422 nm). Ru(bpz)$_3$@InTATB (λ_{em} = 613 nm, λ_{ex} = 443 nm) also showed a slightly blue-shifted PL emission band, compared to Ru(bpz)$_3$@InBTB (λ_{em} = 619 nm, λ_{ex} = 443 nm). Thus, both Ru(phen)$_3$@InTATB and Ru(bpz)$_3$@InTATB showed slightly blue-shifted ^{3}MLCT emission band maxima, compared to Ru(phen)$_3$@InBTB and Ru(bpz)$_3$@InBTB.

Although the crystal structures of RuL_3@InTATB could not be determined in this study, the crystal structures of the three RuL_3@InBTB MOFs have been fully characterized in a previous report.[9] The doubly-interpenetrated anionic framework structure of InTATB is isostructural with InBTB; thus, the differences between the positions of encapsulated $[RuL_3]^{2+}$ ions for the two cases might not be significant. Hence, the differences of PL emission maxima between the RuL_3@InTATB and RuL_3@InBTB systems are attributable to the different functionalities and environments of the channels, due to the presence of N-atom containing triazine rings, except in the case of $[Ru(bpy)_3]^{2+}$. Nevertheless, these differences are insufficient to substantially alter the redox potentials of the corresponding excited Ru(II)* species.

Table S2 (SI) summarizes the time-resolved photoluminescence (TRPL) decay curve parameters for the solid RuL_3@InTATB samples that were measured to compare the excited state lifetimes of the encapsulated $[RuL_3]^{2+}$ species, compared to free ions. The enhanced ^{3}MLCT excited-state lifetimes of the encapsulated $[RuL_3]^{2+}$ ions are believed to contribute to their improved photoredox catalytic activities. The ^{3}MLCT excited-state lifetime of the $[Ru(bpy)_3]^{2+}$ ion is also known to exhibit strong solvent dependence in solution.[31] Therefore, variations in excited-state lifetimes were anticipated for the RuL_3@InTATB MOFs due to their distinct electron-accepting pore environments, as compared to RuL_3@InBTB. The decay profiles are presented in Fig. 5.

We compared the amplitude-average lifetimes rather than the intensity-average lifetimes, as the former generally provided more reliable and representative data in most cases.[35] Both Ru(bpy)$_3$@InTATB and Ru(bpz)$_3$@InTATB showed extended amplitude-average lifetimes, compared to the free $[Ru(bpy)_3]^{2+}$ and $[Ru(bpz)_3]^{2+}$ ions. On the other hand, Ru(phen)$_3$@InTATB showed a slightly reduced amplitude-average lifetime than the free $[Ru(phen)_3]^{2+}$ ion. Interestingly, in the case of the $[Ru(phen)_3]^{2+}$ free ion, its solid-state amplitude-average lifetime (565 ns) is much longer than those of the $[Ru(bpy)_3]^{2+}$ and $[Ru(bpz)_3]^{2+}$ ions. These solid-state data are quite different from the solution-state data. For example, the average lifetimes of all free ions in acetonitrile solution decrease in the order $[Ru(bpy)_3]^{2+}$ > $[Ru(bpz)_3]^{2+}$ > $[Ru(phen)_3]^{2+}$ at 1100 > 740 > 500 ns, respectively.[12] Notably, each RuL_3@InTATB exhibited longer amplitude-average lifetimes compared to the corresponding RuL_3@InBTB. This enhancement in the Ru(II)* excited-state lifetimes may account for the improved photoredox catalytic activities observed in the RuL_3@InTATB systems. In the case of Ru(bpy)$_3$@InTATB (499 ns), the lifetime was enhanced by as much as 79 ns, compared to Ru(bpy)$_3$@InBTB (420 ns). Although in this report, we were unable to solve the crystal structure of Ru(bpy)$_3$@InTATB, the previous crystal structure of Ru(bpy)$_3$@InBTB indicated two very effective simultaneous intermolecular π–π stacking interactions between one of the bpy ligands and the BTB^{3-} linker

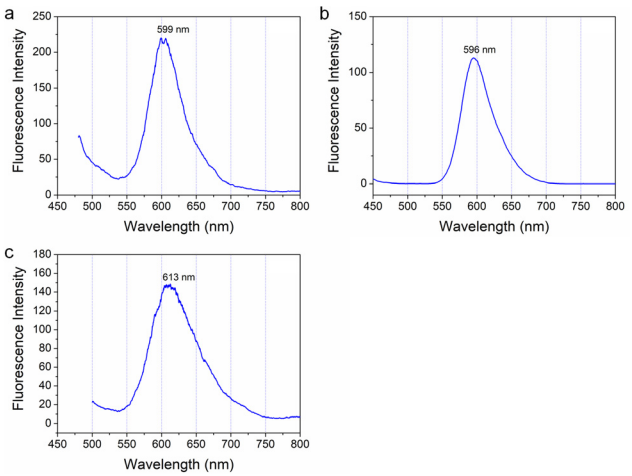

Fig. 4 Solid-state PL spectra of (a) Ru(bpy)$_3$@InTATB (λ_{ex} = 450 nm), (b) Ru(phen)$_3$@InTATB (λ_{ex} = 422 nm), and (c) Ru(bpz)$_3$@InTATB (λ_{ex} = 443 nm).

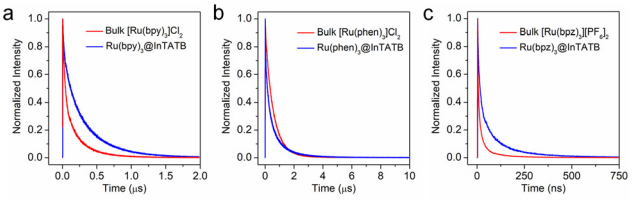

Fig. 5 Normalized PL decay curves for (a) Ru(bpy)$_3$@InTATB and free $[Ru(bpy)_3]Cl_2$, (b) Ru(phen)$_3$@InTATB and free $[Ru(phen)_3]Cl_2$, and (c) Ru(bpz)$_3$@InTATB and free $[Ru(bpz)_3][PF_6]_2$.

(Fig. S2, SI).[9] The two aromatic rings of the bpy ligand separately interact with the central phenyl group and another phenyl group of the BTB^{3-} linker. Thus, strong intermolecular π–π stacking interactions likely occur between one of the bpy ligands and the $TATB^{3-}$ linker in $Ru(bpy)_3$@InTATB. Such interactions may contribute significantly to the pronounced enhancement of its excited-state lifetime. In contrast, in the case of $Ru(phen)_3$@InBTB, only a single intermolecular π–π stacking interaction was observed between a phen ligand and the BTB^{3-} linker.

Table S3 (SI) summarizes the detailed lifetime components extracted from each sample after fitting the decay curves using appropriate exponential models. The tri-exponential curve fitting of $Ru(bpy)_3$@InTATB clearly demonstrates enhanced lifetimes for all three extracted components (τ_1, τ_2, and τ_3) compared to $Ru(bpy)_3$@InBTB. For $Ru(phen)_3$@InTATB, both the fast and slow lifetime components (τ_1 and τ_3) exhibit slightly decreased values compared to those of $Ru(phen)_3$@InBTB. In contrast, the intermediate lifetime component (τ_2) of $Ru(phen)_3$@InTATB is slightly longer than that of $Ru(phen)_3$@InBTB. The tri-exponential curve fitting for $Ru(bpz)_3$@InTATB reveals significantly enhanced lifetime components (τ_1, τ_2, and τ_3) compared to those of $Ru(bpz)_3$@InBTB. Unlike $Ru(bpz)_3$@InBTB, which required a substantial fourth component (τ_4) for accurate fitting, $Ru(bpz)_3$@InTATB was well-described using only three components. Collectively, these results clearly indicate that encapsulated $[RuL_3]^{2+}$ ions in InTATB, with the exception of $[Ru(phen)_3]^{2+}$, exhibit enhanced excited-state lifetimes. Even the $[Ru(phen)_3]^{2+}$ ion in InTATB did not exhibit a significant difference compared to $Ru(phen)_3$@InBTB. While the precise role of the electron-accepting triazine ring in the $TATB^{3-}$ linker requires further investigation, it is clear that simply replacing the central phenyl group of the BTB^{3-} linker with the electron-accepting triazine ring can promote a more stabilized, long-lived charge-separated state in the RuL_3@InTATB system. In contrast to the triazine ring, the phenyl groups in the BTB^{3-} linker are considered electron-donating sites.[36]

Fig. 6 presents fluorescence lifetime imaging microscopy (FLIM) results, clearly confirming the enhanced excited-state lifetimes of both $Ru(bpy)_3$@InTATB and $Ru(bpz)_3$@InTATB compared to their free ions. In contrast, the difference between $Ru(phen)_3$@InTATB and free $[Ru(phen)_3]^{2+}$ appears minimal. A rough estimation of the cation penetration depth can also be inferred from the FLIM image shown in Fig. 6d, with values ranging from 1.2 to 7.1 μm. This penetration depth is comparable to that observed for RuL_3@InBTB. As the cation exchange proceeds, the relatively large $[RuL_3]^{2+}$ ions tend to partially block the mesoscale pores, resulting in shallower penetration depths.

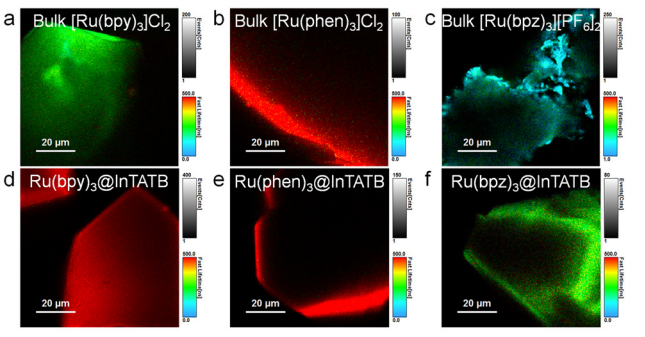

Fig. 6 Fluorescence lifetime imaging microscopy (FLIM) images of (a) free $[Ru(bpy)_3]Cl_2$, (b) free $[Ru(phen)_3]Cl_2$, (c) free $[Ru(bpz)_3][PF_6]_2$, (d) $Ru(bpy)_3$@InTATB, (e) $Ru(phen)_3$@InTATB, and (f) $Ru(bpz)_3$@InTATB.

3.3. FT-IR and CV studies

To further confirm the successful encapsulation of $[RuL_3]^{2+}$ ions within InTATB, FT-IR spectroscopy was performed. The FT-IR spectra of the three RuL_3@InTATB samples showed slight differences compared to that of the as-prepared InTATB (Fig. S3, SI). These minor variations likely arise from the overlapping aromatic signals of the InTATB framework and the polypyridine ligands of the encapsulated $[RuL_3]^{2+}$ ions. Nevertheless, certain signals observed from the as-prepared InTATB disappeared for RuL_3@InTATB. These FT-IR results further confirm the successful encapsulation of $[RuL_3]^{2+}$ ions.

Table S4 (SI) summarizes the redox potentials of the Ru(II) species in $Ru(bpy)_3$@InTATB that were estimated by cyclic voltammetry (CV, Fig. S4, SI) and fluorescence spectroscopy. The redox potentials of the excited state Ru(II)* species were calculated based on the literature method.[32–34] Like the previous $Ru(bpy)_3$@InBTB, the Ru(II) polypyridine species in $Ru(bpy)_3$@InTATB displayed slightly different redox potentials, compared with the values measured for free ions in solution. These results suggest that encapsulation within the InTATB channels does not significantly alter the intrinsic redox properties of the Ru(II) polypyridine species. Instead, the electron-accepting environment of the InTATB channels primarily contributes to the enhancement of the excited-state lifetimes, rather than affecting the redox potentials of the encapsulated $[RuL_3]^{2+}$ ions.

3.4. Visible-light photoredox catalysis

Fig. 7 presents the aza-Henry reaction between THIQ and nitromethane, as well as the aerobic oxidation of benzyl halides, both selected as model visible-light photoredox reactions catalyzed by RuL_3@InTATB, functioning as a single electron-transfer (SET) photocatalyst.[12] The aza-Henry reaction, also known as the nitro-Mannich reaction, is a versatile synthetic method that involves the addition of a nitroalkane to an imine, yielding β-nitroamines.[37] The aza-Henry reaction of THIQ was proven to be effectively catalyzed by RuL_3@MOF including RuL_3@InBTB under visible-light irradiation using a household fluorescent lamp under aerobic conditions at RT.[9,18] Although the UV light from a commercial fluorescent lamp is largely blocked by the phosphor coating inside the lamp, a small amount of UV radiation may still be emitted. The three heterogenized RuL_3@InTATB catalysts were tested under the same reaction conditions. As seen in Fig. 8a, all RuL_3@InTATB samples exhibited much higher desired

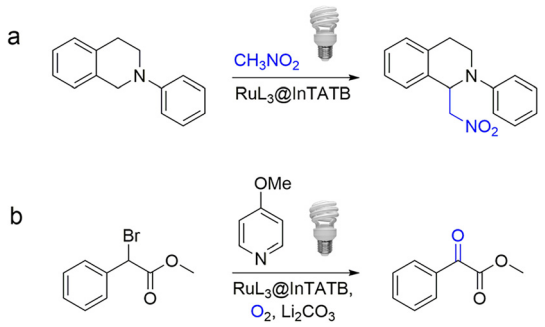

Fig. 7 The aza-Henry reaction of THIQ with nitromethane (a) and aerobic oxidation of methyl α-bromophenylacetate (b) catalyzed by RuL_3@InTATB visible-light photoredox catalytic systems in air.

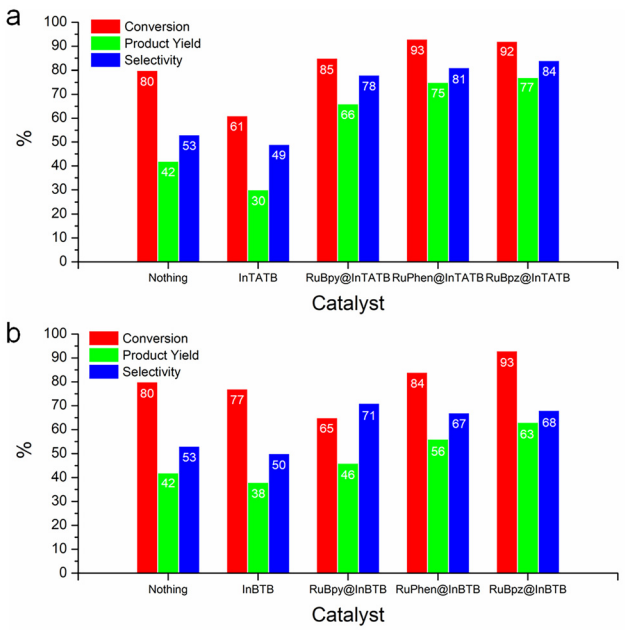

Fig. 8 Comparison of the catalytic activities of RuL_3@InTATB (a) and RuL_3@InBTB (b) for the aza-Henry reaction of THIQ under the same reaction conditions. The data for RuL_3@InBTB in panel (b) are from the literature.[9]

product yields, as well as conversions, than the control experiments without catalysts or with the as-prepared InTATB. The as-prepared InTATB showed a low product yield of only 30%, like the as-prepared InBTB (38%). These data do not significantly differ from the control experiment without catalysts (42%). Therefore, the as-prepared InTATB cannot be regarded as an effective catalyst. While the conversion and product yield of $Ru(bpy)_3$@InTATB were 85 and 66%, the corresponding values for $Ru(bpy)_3$@InBTB were 65 and 46%, respectively. The product selectivity of $Ru(bpy)_3$@InTATB is much higher than that of $Ru(bpy)_3$@InBTB. Notably, both $Ru(phen)_3$@InTATB and $Ru(bpz)_3$@InTATB showed very high conversions of 93 and 92% and product yields of 75 and 77%. Thus, the desired product selectivity values for $Ru(phen)_3$@InTATB and $Ru(bpz)_3$@InTATB were 81 and 84%, respectively. These catalytic activities are much superior to those of the corresponding RuL_3@InBTB. In fact, various byproducts or side products can be generated, primarily consisting of unreacted imine and some oligomerized species derived from the imine. Although we did not perform a detailed analysis of these byproducts, the product selectivity in our system is not considered low, as evidenced by the results shown in Fig. 8 for the RuL_3@InTATB systems.

We speculate that the enhanced excited state lifetimes of $[RuL_3]^{2+}$ ions in RuL_3@InTATB due to the electron-accepting triazine group within InTATB may play an important role in enhancing the catalytic activities of RuL_3@InTATB, compared to RuL_3@InBTB. Fig. S5 (SI) shows the proposed mechanism of the aza-Henry reaction based on the previous report.[12] Based on this mechanism, the $[RuL_3]^{2+}$ ions in RuL_3@InTATB, with their elongated excited-state lifetimes, can more efficiently react with THIQ, thereby facilitating the overall reaction. Importantly, the third step of the reductive quenching cycle involves the reduction of O_2 by $[RuL_3]^{+}$@InTATB to generate the superoxide anion radical ($O_2^{\bullet-}$) and to regenerate RuL_3@InTATB. The resulting superoxide anion radical subsequently abstracts a hydrogen atom from the aminium radical cation derived from THIQ. Therefore, the use of ambient air as the O_2 source is more cost-effective than conventional catalytic systems, which typically require pure O_2 and elevated temperatures above RT.[38]

The recyclability of the $Ru(bpy)_3$@InTATB catalyst in the aza-Henry reaction was evaluated over three consecutive recycling tests, which showed that the catalyst retained a moderate level of its original activity (Fig. S6 (SI); product yields: 1st cycle, 62%; 2nd, 59%; 3rd, 49%), indicating good robustness. The gradual decrease in yield was partly attributed to minor catalyst loss during the recovery process. Remarkably, a $Ru(bpy)_3$@InTATB sample prepared one and a half years earlier maintained its catalytic performance. This sample had been stored in a capped vial under ambient conditions without an inert atmosphere, demonstrating that long-term storage on a standard laboratory shelf is practical.

The aerobic oxidation of benzyl halides, or α-aryl halogen compounds, to produce α-aryl carbonyl derivatives has also been catalyzed by visible-light PCs in the presence of an auxiliary organocatalyst, such as 4-methoypyridine, at RT. Interestingly, to generate a substrate-based radical species, this reaction requires both the visible-light PC, and a suitable organocatalyst. An additional base was also required to prevent the protonation of 4-methoypyridine during the reaction.[28,39] Ru(II) polypyridine compounds are active visible-light PCs for this reaction in air. Fig. S7 (SI) shows the proposed reaction mechanism based on the previously suggested reaction mechanism for the free $[Ru(bpy)_3]^{2+}$ ion.[39] This mechanism indicates that the photoexcited $[*Ru(bpy)_3]^{2+}$ ion acts as an oxidant instead of a reductant and reduces to $[Ru(bpy)_3]^{+}$. The superoxide anion radical oxidizes to O_2 in this reductive quenching cycle of $[*Ru(bpy)_3]^{2+}$. The subsequent SET event transfers an electron from $[Ru(bpy)_3]^{+}$ to 4-methoxypyridinium salt, generated between 4-methoxypyridine and ethyl α-bromophenylacetate, to produce the corresponding

dihydropyridyl radical. All three RuL_3@InTATB samples showed good catalytic activities, as summarized in Table S5 (SI). Among the three PCs, Ru(phen)$_3$@InTATB exhibited the highest catalytic activities across all five tested substrates, delivering product yields in the range of 71–95%. In comparison, Ru(bpy)$_3$@InTATB showed slightly lower yields ranging from 58 to 76%, while Ru(bpz)$_3$@InTATB gave the lowest yields, ranging from 33 to 77%, relative to both Ru(phen)$_3$@InTATB and Ru(bpy)$_3$@InTATB.

4. Conclusions

We prepared three new heterogeneous visible-light photoredox catalytic systems (RuL_3@InTATB) through the encapsulation of cationic Ru(II) polypyridine complexes within the mesoscale channels of an anionic InTATB MOF having strong electron acceptor sites in mesoscale pores. The PL properties of the RuL_3@InTATB systems were investigated by fluorescence spectroscopy and TRPL decay measurements. Ru(bpy)$_3$@InTATB and Ru(bpz)$_3$@InTATB both exhibited extended PL lifetimes, compared to free ions and the corresponding RuL_3@InBTB. These enhanced lifetimes can be attributed to the confinement effect and the presence of electron-accepting sites within the framework. In particular, the $TATB^{3-}$ linker of InTATB can interact effectively with one of the three bpy ligands of the $[Ru(bpy)_3]^{2+}$ ion through intermolecular π–π interactions. This makes InTATB a more ideal MOF host for Ru(II) polypyridine PCs to stabilize the ^{3}MLCT-based excited state of Ru(II)* polypyridine PCs, compared to the isostructural InBTB containing a central phenyl group. The visible-light photoredox catalytic reaction, aza-Henry reaction of THIQ, did indeed indicate the superior catalytic activities of the RuL_3@InTATB systems over the RuL_3@InBTB systems. The desired product selectivity was also enhanced. The RuL_3@InTATB systems were also active for the aerobic oxidation of benzyl halides under visible light at RT. These results clearly suggest that fine-tuning the pore environment of MOFs to suit the encapsulated PCs can favorably enhance their photoredox catalytic activity. Furthermore, RuL_3@InTATB represents an effective heterogeneous visible-light photoredox catalytic system. We envision that appropriate pore engineering of MOF hosts could improve the photoredox catalytic performance of a wide range of transition metal-based PCs and sensitizers, including cost-effective, earth-abundant metal complexes.[14,40]

Conflicts of interest

The authors have no conflicts of interest to disclose.

Data availability

The data supporting this article have been included as part of the SI: encapsulation amounts, PL lifetimes and their components, redox potentials, catalysis results, microscopy images, crystal structures, FT-IR spectra, cyclic voltammograms, and proposed reaction mechanisms. See DOI: https://doi.org/10.1039/d5dt01373a.

Acknowledgements

This work was supported by grants (2022R1F1A1063615) of the Basic Science Research Program through the National Research Foundation (NRF) funded by the Ministry of Education, Science and Technology, Republic of Korea.

References

1 V. Ramamurthy, *Chem. Commun.*, 2022, **58**, 6571–6585.
2 A. M. Rice, C. R. Martin, V. A. Galitskiy, A. A. Berseneva, G. A. Leith and N. B. Shustova, *Chem. Rev.*, 2020, **120**, 8790–8813.
3 M. Gutiérrez, Y. Zhang and J.-C. Tan, *Chem. Rev.*, 2022, **122**, 10438–10483.
4 H.-Q. Yin and X.-B. Yin, *Small*, 2022, **18**, 2106587.
5 E.-Y. Cho, J.-M. Gu, I.-H. Choi, W.-S. Kim, Y.-K. Hwang, S. Huh, S.-J. Kim and Y. Kim, *Cryst. Growth Des.*, 2014, **14**, 5026–5033.
6 I.-H. Choi, S. B. Yoon, S. Huh, S.-J. Kim and Y. Kim, *Sci. Rep.*, 2018, **8**, 9838.
7 S. Yoon, H.-C. Kim, Y. Kim and S. Huh, *Bull. Korean Chem. Soc.*, 2021, **42**, 326–332.
8 G. Kuzmanich, S. Simoncelli, M. N. Gard, F. Spänig, B. L. Henderson, D. M. Guldi and M. A. Garcia-Garibay, *J. Am. Chem. Soc.*, 2011, **133**, 17296–17306.
9 I.-H. Choi, S. Yoon, S. Huh, S.-J. Kim and Y. Kim, *Chem. – Eur. J.*, 2020, **26**, 14580–14584.
10 J. M. R. Narayanam and C. R. J. Stephenson, *Chem. Soc. Rev.*, 2011, **40**, 102–113.
11 T. P. Yoon, *ACS Catal.*, 2013, **3**, 895–902.
12 C. K. Prier, D. A. Rankic and D. W. C. MacMillan, *Chem. Rev.*, 2013, **113**, 5322–5363.
13 L. Qian and M. Shi, *Chem. Commun.*, 2023, **59**, 3487–3506.
14 O. S. Wenger, *J. Am. Chem. Soc.*, 2018, **140**, 13522–13533.
15 A. A. Yakushev, A. S. Abel, A. D. Averin, I. P. Beletskaya, A. V. Cheprakov, I. S. Ziankou, L. Bonneviot and A. Bessmertnykh-Lemeune, *Coord. Chem. Rev.*, 2022, **458**, 214331.
16 B. Tambosco, K. Segura, C. Seyrig, D. Cabrera, M. Port, C. Ferroud and Z. Amara, *ACS Catal.*, 2018, **8**, 4383–4389.
17 C. Wang, Z. Xie, K. E. deKrafft and W. Lin, *ACS Appl. Mater. Interfaces*, 2012, **4**, 2288–2294.
18 J. Pang, S. Yuan, J.-S. Qin, C. T. Lollar, N. Huang, J. Li, Q. Wang, M. Wu, D. Yuan, M. Hong and H.-C. Zhou, *J. Am. Chem. Soc.*, 2019, **141**, 3129–3136.
19 H. Lv, C. Ma, Z. Zhu, Q.-H. Li, S. Chen, F. Wang and S. Li, *J. Solid State Chem.*, 2023, **322**, 123948.
20 J. M. Mayers, L. Wojtas and R. W. Larsen, *Eur. J. Inorg. Chem.*, 2023, **26**, e202300088.

21 D. Micheroni, Z. Lin, Y.-S. Chen and W. Lin, *Inorg. Chem.*, 2019, **58**, 7645–7648.
22 N. Linares, E. Serrano, M. Rico, A. M. Balu, E. Losada, R. Luque and J. García-Martínez, *Chem. Commun.*, 2011, **47**, 9024–9035.
23 S. Huh, J. W. Wiench, J.-C. Yoo, M. Pruski and V. S.-Y. Lin, *Chem. Mater.*, 2003, **15**, 4247–4256.
24 Y. Kim and S. Huh, *CrystEngComm*, 2016, **18**, 3524–3550.
25 Y. Huang, Z. Lin, H. Fu, F. Wang, M. Shen, X. Wang and R. Cao, *ChemSusChem*, 2014, **7**, 2647–2653.
26 Y. Lee, S.-J. Woo, J.-J. Kim and J.-I. Hong, *Dyes Pigm.*, 2020, **172**, 107864.
27 Q. Liao, W. Xu, X. Huang, C. Ke, Q. Zhang, K. Xi and J. Xie, *Sci. China: Chem.*, 2020, **63**, 707–714.
28 W. Liu, Y. Yang, X. Yang, Y.-L. Peng, P. Cheng, Z. Zhang and Y. Chen, *ACS Appl. Mater. Interfaces*, 2021, **13**, 58619–58629.
29 Z. Li and C.-J. Li, *J. Am. Chem. Soc.*, 2005, **127**, 6968–6969.
30 D. M. Arias-Rotondo and J. K. McCusker, *Chem. Soc. Rev.*, 2016, **45**, 5803–5820.
31 J. V. Caspar and T. J. Meyer, *J. Am. Chem. Soc.*, 1983, **105**, 5583–5590.
32 C. Creutz and N. Sutin, *Inorg. Chem.*, 1976, **15**, 496–499.
33 C. R. Bock, J. A. Connor, A. R. Gutierrez, T. J. Meyer, D. G. Whitten, B. P. Sullivan and J. K. Nagle, *J. Am. Chem. Soc.*, 1979, **101**, 4815–4824.
34 D. W. Thompson, A. Ito and T. J. Meyer, *Pure Appl. Chem.*, 2013, **85**, 1257–1305.
35 A. Sillen and Y. Engelborghs, *Photochem. Photobiol.*, 1998, **67**, 475–486.
36 K. P. Goetz, D. Vermeulen, M. E. Payne, C. Kloc, L. E. McNeil and O. D. Jurchescu, *J. Mater. Chem. C*, 2014, **2**, 3065–3076.
37 V. K. Patel, D. P. Patel and S. K. Singh, *Tetrahedron*, 2025, **185**, 134803.
38 G. Y. Go, R. P. S. Rajan, S. Lee and H. C. Choi, *Mol. Catal.*, 2024, **552**, 113681.
39 Y. Su, L. Zhang and N. Jiao, *Org. Lett.*, 2011, **13**, 2168–2171.
40 W. Nam, Y.-M. Lee and S. Fukuzumi, *Bull. Korean Chem. Soc.*, 2024, **45**, 503–519.